Engineering Applications of Artificial Intelligence 43 (2015) 27–34

Contents lists available at ScienceDirect

Engineering Applications of Artificial Intelligence

journal homepage: www.elsevier.com/locate/engappai

A hierarchical airlight estimation method for image fog removal

Fan-Chieh Cheng, Chung-Chih Cheng, Po-Hsiung Lin, Shih-Chia Huang *

Department of Electronic Engineering, National Taipei University of Technology, Taipei 10608, Taiwan

ARTICLE INFO

Article history:
Received 20 July 2014
Received in revised form
5 March 2015
Accepted 22 March 2015
Available online 26 April 2015

Keywords:
Defogging
Physical optic model
Airlight estimation

ABSTRACT

Fog phenomena result in airlight generation and degrade the visibility of the color image captured from the camera. To improve visibility, airlight estimation is necessary for image fog removal. As airlight is very bright, the traditional methods directly select bright pixels for airlight estimation. However, some bright pixels generated by light sources, such as train headlights, may interfere with the accuracy of the above-mentioned methods. In this paper, we propose a new airlight estimation method. Based on Gaussian distribution, the proposed method selects the airlight candidates in the brightest region of the input image. Moreover, the color similarity estimation is also applied to hierarchically refine the candidates. We then compute the average color from the refined candidate pixels for airlight estimation. Experimental results demonstrate that the proposed method is more accurate than other airlight estimation methods and has low time complexity.

1. Introduction

In foggy weather, visibility degradation occurs when observers perceive object light blended with airlight due to scattering caused by a medium in the atmosphere, such as small water droplets. Degraded visibility in a foggy image then affects the effect of computer vision techniques, including motion detection (Kim and Kim, 2012), face tracking (Zou et al., 2013), license plate recognition (Wen et al., 2011), and so on. Hence, for multimedia devices, such as advanced driver assistance (Hautiere et al., 2010) and video surveillance (Yoon et al., 2012) systems, fog removal techniques play an important role for improving the visibility of the images.

According to the literature (Narasimhan and Nayar, 2003a), image defogging can be performed by modifying the distribution of the image histogram, but the effect is usually limited. As the haze formation was modeled using Koschmieder's law, numerous defogging methods based on this optical model were disclosed in the field. Basically, those methods can be divided into two groups: non-single image information methods (Narasimhan and Nayar, 2003a; Shwartz et al., 2006; Kopf et al., 2008) and single image information methods (Tan, 2008; Fattal, 2008; He et al., 2011; Gibson et al., 2012; Cheng et al., 2012; Shiau et al., 2013).

Fog removal methods using non-single image information include the use of multiple images or additional information, such as camera settings. On the other hand, fog removal methods developed using the single image require the reasonable assumption and accurate prior during image processing. However, when processing the single input image, the use of single image information is often more convenient than the use of non-single image information. Therefore, development focus concerning defogging methods in recent years has increasingly oriented towards the use of single image information.

Upon comparing the visibility of fog-free images to that of foggy images, the former visibly held local contrast, whereas the latter only faintly held local contrast. Hence, maximization of the local contrast was focused on in order to develop the visibility enhancement method (Tan, 2008). Although foggy effects of input images can be improved by enhancing the visibility, over-enhancement may occur locally.

In the fog estimation model, Fattal (2008) made an assumption that the propagation of light projected and the surface shading are partially uncorrelated. According to this assumption, mathematical statistics were utilized to estimate the albedo of a scene and infer the transmission medium, after which the fog formation in the degraded image can be removed. However, satisfactory restoration results cannot be produced via the use of Fattal's method if degraded images include heavy fog formation.

He et al. designed their fog removal method to include airlight estimation and transmission model modules (He et al., 2011). After collecting statistical information, they found that the general pixels usually feature very low luminance, with fog pixels contributed by airlight. Therefore, dark channel prior (DCP) was developed for airlight estimation, and it also transforms to the transmission model via negative computation. However, halo artifacts are usually caused by DCP that need to be further refined (He et al., 2011).

* Corresponding author.
E-mail address: schuang@ntut.edu.tw (S.-C. Huang).

http://dx.doi.org/10.1016/j.engappai.2015.03.011
0952-1976/

In general, airlight estimation can be performed by manual and automatic methods. The manual method directly defines image regions affected by airlight (Narasimhan and Nayar, 2003b), but it is inapplicable for realistic application due to frequent interruption. In contrast, the automatic methods are more convenient. Thus, we estimate airlight in single images automatically (He et al., 2011; Gibson et al., 2012; Cheng et al., 2012; Shiau et al., 2013). However, the traditional methods select only bright pixels as candidates of airlight regions (He et al., 2011; Gibson et al., 2012; Cheng et al., 2012; Shiau et al., 2013). This means that if bright pixels generated by light sources exist in the input images, those methods may select inappropriate candidates that result in wrong airlight estimation. In this paper, we focus solely on the challenge of accurate airlight estimation.

The remainder of this paper is divided as follows: Section 2 describes the physics-based optical model, four modern fog removal methods, and the motivation behind the proposed method. In Section 3, the proposed method is described in detail. Section 4 shows experimental results that present the comparison between ours and several other state-of-the-art defogging methods. Finally, we conclude this paper and present future work in Section 5.

2. Related works

According to Middleton (1952), the physics-based optical model can be employed for defogging. In general, object color corresponds to the light reflected from an object. The perceived object color is degraded if the reflected light partially transmits from fog to observer. Let L_0 be the reflected light of an object and L_∞ be ambient light. The presented light of object L can be formulated by

$$L = L_0 e^{-\beta d} + L_\infty (1 - e^{-\beta d}), \tag{1}$$

where $e^{-\beta d}$ is the fog factor that reveals a light reinforcement of object $L_0 e^{-\beta d}$ and airlight $L_\infty(1-e^{-\beta d})$.

In the optical model, the pixel value I can be computed using the optical model denoted by

$$I = f(L_0 e^{-\beta d} + L_\infty (1 - e^{-\beta d})). \tag{2}$$

Note that the conversion process between the incident energy on the imaging sensor and the generated pixels of the image is assumed to be linear in this form. Hence, the above formula is modified as

$$\begin{aligned} I &= f(L_0 e^{-\beta d}) + f(L_\infty (1 - e^{-\beta d})) \\ &= f(L_0) e^{-\beta d} + f(L_\infty)(1 - e^{-\beta d}) \\ &= R e^{-\beta d} + A_\infty (1 - e^{-\beta d}), \end{aligned} \tag{3}$$

When the atmosphere is homogeneous, $e^{-\beta d}$ can be represented by the transmission model t. For each pixel x, Eq. (3) is then approximated as

$$I_c(x) = R_c(x) t(x) + A_c (1 - t(x)), \tag{4}$$

where I_c is the original RGB values, R_c is the restored RGB values, A_c is the airlight values, and t is the transmission value. Note that $c = 0, 1, 2$ denotes red, green, and blue values, respectively. The fog removal methods then compute A_c and t, after which R_c can be further restored from I_c (He et al., 2011; Gibson et al., 2012; Cheng et al., 2012; Shiau et al., 2013).

We then briefly review four modern fog removal methods based on Eq. (3), including DCP, Median-DCP (MDCP), Lowest-level Channel Prior (LCP), and Edge Preservation Haze Removal (EPHR), which all include an airlight estimation module and a transmission model module. Note that DCP, MDCP, and LCP methods employ the same airlight estimation module, which is mentioned in Section 2.1.

2.1. DCP method

It is necessary to generate the dark channel of the input image before airlight estimation and transmission modeling (He et al., 2011). Let $I_{\min}$ be the minimum channel that involves the lowest color value per pixel. The minimum channel is formulated by

$$I_{\min}(x) = \min_{c \in [0,2]} (I_c(x)). \tag{5}$$

After the local patch Ω is defined, the dark channel is computed by

$$I'_{\min}(x) = \min_{p \in \Omega(x)} (I_{\min}(p)), \tag{6}$$

where p is an arbitrary pixel in the local patch. According to He et al. (2011), Ω can be 3×3, 15×15, or 31×31. However, in different cases, Ω should be manually adjusted to generate the optimized output image.

The DCP method then picks up the top 0.1% bright pixels of $I'_{\min}$ as candidates for airlight estimation. Suppose that $M(x) = 1$ for the selected candidates and $M(x) = 0$ for non-candidates; airlight color A_c can be computed by Algorithm 1.

Algorithm 1. Airlight estimation of DCP algorithm.

```
(A0, A1, A2) ← (0, 0, 0)
for each pixel x do
  if M(x) = 1 then
    for c ← 0 to 2 do
      if Ic(x) > Ac then
        Ac ← Ic
      end if
    end for
  end if
end for
```

In addition to airlight estimation, $I'_{\min}$ is also used in the transmission model module. For each pixel x, the transmission model is formulated as follows:

$$t(x) = 1 - \omega \left(\frac{I'_{\min}(x)}{\max(I'_{\min})} \right), \tag{7}$$

where ω is a pre-defined parameter fixed by 0.95. However, Eq. (8) often generates block artifacts. Since Eq. (3) has a similar form as the image matting equation (He et al., 2011):

$$\mathbf{I} = \mathbf{F}\alpha + \mathbf{B}(1 - \alpha), \tag{8}$$

where α is the foreground opacity, $\mathbf{F}$ and $\mathbf{B}$ are foreground and background colors, respectively, and a soft matting method (Levin et al., 2008) is employed to refine t(He et al., 2011). After generating A_c and t, we can use Eq. (4) for fog removal.

2.2. MDCP method

The MDCP method directly employs the airlight estimation of DCP, but it modifies the transmission model of DCP (Gibson et al., 2012). To avoid the high computation cost of soft matting (He et al., 2011), the MDCP method uses median filter for adjusting Eq. (8). Instead of the minimum filter, the median filter is employed for processing each pixel of $I_{\min}$.

The estimated transmission t of the MDCP method is then modified from Eq. (8) and can be formulated by

$$t(x) = 1 - \omega \left(\frac{I'_{\text{med}}(x)}{\max(I'_{\text{med}})} \right), \tag{9}$$

where

$$I'_{\text{med}}(x) = \operatorname*{med}_{p \in \Omega(x)} (I_{\min}(p)). \tag{10}$$

According to Gibson et al. (2012), Eq. (8) generates halo effects of t if there is one object pixel at the extreme neighborhood edges. However, Eq. (9) can effectively reduce this problem.

2.3. LCP method

For airlight estimation, the LCP method also uses the same module of DCP. To present an alternative strategy for the transmission model of DCP, the LCP method (Cheng et al., 2012) uses the minimum channel (Eq. (5)) instead of the dark channel (Eq. (6)).

In order to preserve the local texture of the input color image, a fast $O(1)$ bilateral filter proposed in Chaudhury et al. (2011) is employed. Compared to the traditional bilateral filter visiting each pixel intensity of the local window, the $O(1)$ version simply employs the complex exponentials to weight each intensity, which means that no local window is needed during the process. Let $j\gamma$ be the weight factor. The filter process of $I_{\min}$ is then formulated as follows:

$$I_{avg}(x) = \frac{\sum_{n \le N} d_n(x)\overline{g_n}(x)}{\sum_{n \le N} d_n(x)\overline{h_n}(x)}, \tag{11}$$

where $h_n(x)$ is determined by $\exp(jn\gamma I_{\min}(x))$ and $g_n(x) = I_{\min}(x)h_n(x)$. The transmission t is then computed by

$$t(x) = 1 - \frac{I_{avg}(x)}{\max(I_{avg})}. \tag{12}$$

2.4. EPHR method

For the practical image processing applications, the EPHR method that is an approximation of He et al. (2011) includes the simplified airlight estimation and transmission model (Shiau et al., 2013). After defogging, a simple saturation correction using exponential computation is further conducted to obtain a visually pleasant result (Shiau et al., 2013).

Compared to the DCP, MDCP, and LCP methods that find the top 0.1% bright pixels, the EPHR method directly selects the maximum value of the dark channel to estimate the atmospheric light. Let s be the pixel index of the maximum luma of the dark channel. With the weighting parameter set to 0.875, the simplified atmospheric light is estimated by

$$A_c = 0.875 \times I_c(s), \tag{13}$$

To construct the transmission model efficiently, gradient detection is applied as the pre-process. The detection value $ED(x) = 2$ when the difference of diagonal neighbor pixels is greater than 80, and $ED(x) = 1$ when the difference of vertical neighbor pixels is greater than 80; otherwise, $ED(x) = 0$ for labeling the non-edge pixel. According to the decision of $ED(x)$, t is computed as

$$t(x) = 1 - 0.9375 \times \min_{c \in [0,2]} \left(\frac{P_c^{ED(x)}(x)}{A_c} \right), \tag{14}$$

where $P_c^{ED(x)}(x)$ is the average value. The $P_c^0(x)$ is averaged from the center and 8-neighbor pixels. The $P_c^1(x)$ is averaged from double 4-neighbor, quadruple center, and other four diagonal pixels. The $P_c^2(x)$ is averaged from the double diagonal, quadruple center, and 4-neighbor pixels. When the R_c is restored, the saturation correction is performed by

$$\tilde{R}_c(x) = A_c^{0.3} \times (R_c(x))^{0.7}. \tag{15}$$

2.5. Summary

Although the state-of-the-art methods work well for estimating the transmission model t, airlight estimation using DCP often fails since these methods only consider bright pixels as candidates for foggy ones. Note that the LCP and MDCP methods do not modify the airlight estimation of the DCP and simply improve the transmission module. When the selected candidates include bright pixels generated by light sources, such as headlights, it results in wrong airlight estimation. Although the EPHR method uses the pre-defined parameter to partially reduce this problem, minor side effects may be caused since it does not belong to the automatic design and so is not suitable for advanced vision systems associated with artificial intelligence. To overcome this weakness, this paper proposes a Hierarchical Airlight Estimation (HAE) method that selects as precise candidates only fog pixels and not bright pixels generated by light sources.

As mentioned above, MDCP, LCP, and EPHR are three representative methods in this field. More specifically, they can be further classified as two airlight estimation and three transmission estimation methods. As listed in Table 1, the proposed HAE method is then used to replace the airlight estimation of each method for improvement.

Table 1
Overview of each method.

Modules	MDCP	MDCP-HAE	LCP	LCP-HAE	EPHR	EPHR-HAE
Airlight estimation	DCP	HAE	DCP	HAE	EPHR	HAE
Transmission estimation	MDCP	MDCP	LCP	LCP	EPHR	EPHR

3. Proposed method

Basically, the proposed HAE method has two characteristics:

1. It computes the color probability to select precise candidates for airlight estimation.
2. It does not construct the dark channel before airlight estimation.

The HAE method is designed using YCbCr color space. There are two good points of YCbCr. First, YCbCr is a standard format in various video and image codecs, so that the additional color space conversion is unnecessary. Second, it includes Cb and Cr channels appropriate to chroma evaluation. Thus, we choose YCbCr for developing our method.

Fig. 1 shows the flowchart of the HAE method. Compared to previous methods that use patch-wise processing to estimate the luminance of input images based on Eq. (6) (He et al., 2011; Gibson et al., 2012; Cheng et al., 2012; Shiau et al., 2013), the HAE method analyzes luma and chroma by bright region estimation and color similarity estimation along with pixel-wise processing. Hence, the HAE method can avoid the color distortion of A_c as well as reduce the computation time.

3.1. Bright region estimation

In image processing, histograms are widely used for thresholding (Otsu et al., 1979). As such, we construct the luma histogram to determine bright regions of the input image. Let Y be the luma channel of YCbCr color space for the input image I_c. The histogram of Y is generated by the probability density function (pdf) expressed below:

$$H_Y(y \mid Y_{\min} \le y \le Y_{\max}) = pdf(Y), \tag{16}$$

where $Y_{\min}$ is the minimum value of Y, $Y_{\max}$ is the maximum value of Y, and y is an arbitrary value of Y.

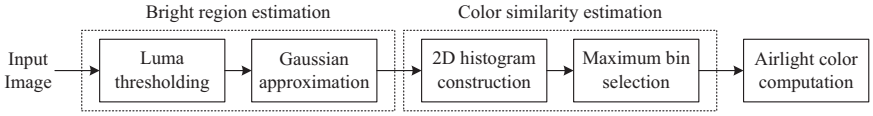

Fig. 1. The flowchart of our HAE method.

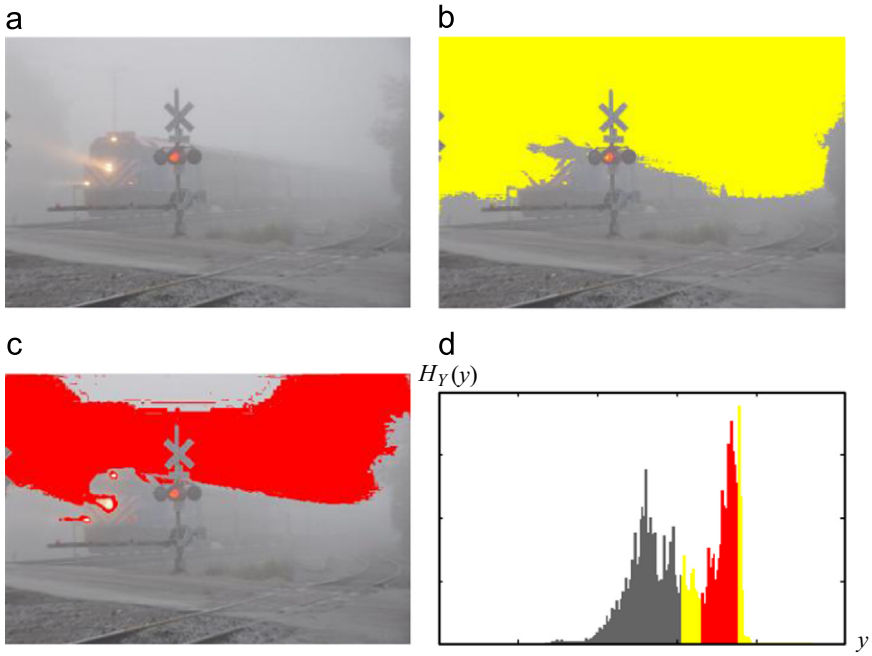

Fig. 2. Illustration bright region estimation: (a) original image; (b) luma thresholding; (c) Gaussian approximation; (d) luma histogram H_Y. (For interpretation of the references to color in this figure caption, the reader is referred to the web version of this article.)

3.1.1. Luma thresholding

In this paper, we simply compute the mean luma value of the input image to determine the rough candidates for fog pixels. The mean luma value is computed as follows:

$$\mu = \frac{\sum_{y=Y_{\min}}^{Y_{\max}} H_Y(y)y}{\sum_{y=Y_{\min}}^{Y_{\max}} H_Y(y)}. \tag{17}$$

For each pixel of the input image, it is selected as a rough candidate if its luma value is greater than μ.

3.1.2. Gaussian approximation

According to the three-σ-rule of Gaussian distribution, most of the values drawn from a Gaussian distribution are limited within one standard deviation away from the mean. Therefore, we further compute local mean and local standard deviation of the rough candidates to select the significant ones.

Let μ' and σ' be the local mean and local standard deviation, respectively. After selecting rough candidates by luma thresholding, μ' and σ' are calculated by

$$\mu' = \frac{\sum_{y=\mu}^{Y_{\max}} H_Y(y)y}{\sum_{y=\mu}^{Y_{\max}} H_Y(y)}, \tag{18}$$

$$\sigma' = \sqrt{\frac{\sum_{y=\mu}^{Y_{\max}} H_Y(y)(y-\mu')^2}{\sum_{y=\mu}^{Y_{\max}} H_Y(y)}}. \tag{19}$$

If the luma value of the rough candidate does not lie within $[\mu'-\sigma', \mu'+\sigma']$, it is removed as a non-candidate pixel.

Fig. 2 shows one example of bright region estimation. Note that the labeled yellow pixels and yellow bins of the luma histogram represent the rough candidates selected by luma thresholding, while the labeled red pixels and red bins of luma histogram represent those refined by Gaussian approximation. Although the yellow region covers the most of the fog pixels in the input image, the non-fog pixels generated by train headlights are also included. After Gaussian approximation, most of the bright pixels of the candidates that correspond to headlights can be removed.

3.2. Color similarity estimation

When the refined candidates are selected by bright region estimation, their chroma values are estimated to fit the color similarity of the most representative fog pixels. Let Cb and Cr be the chroma channels of YCbCr color space for the input image I_c. We then compute the absolute difference of chroma per pixel, which can be expressed as follows:

$$\Delta(x) = |\,\mathrm{Cb}(x) - \mathrm{Cr}(x)\,|\,. \tag{20}$$

3.2.1. 2D histogram construction

In order to estimate the similarity of the candidate pixels, we construct a 2-D histogram that involves luma and chroma information. Suppose that $\Delta_{\max}$ is the maximum absolute difference of chroma and Y_{length} equals $Y_{\max} - Y_{\min} + 1$. The 2-D histogram H_{2D} can be constructed by Algorithm 2.

Algorithm 2. 2D histogram construction.

1: Set H_{2D} to be a $Y_{length} \times (\Delta_{\max}+1)$ zero array
2: **for** each pixel x **do**
3: **if** $Y(x) \geq \mu' - \sigma'$ and $Y(x) \leq \mu' + \sigma'$ **then**

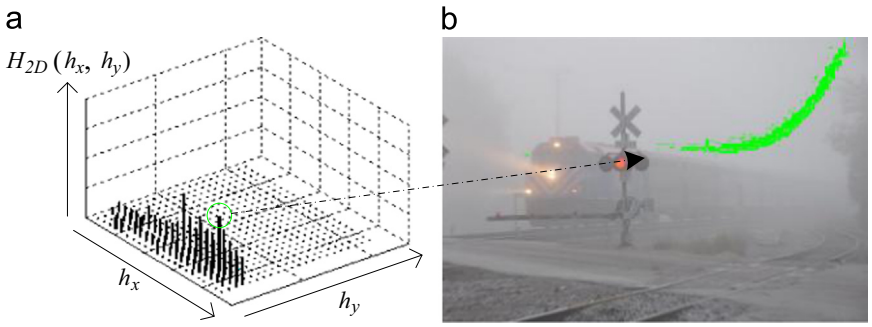

Fig. 3. The illustration of color similarity estimation: (a) 2D histogram H_{2D}; (b) the maximum bin corresponding to the final candidate region. (For interpretation of the references to color in this figure caption, the reader is referred to the web version of this article.)

```
        h_x ← Y(x) − (μ′ − σ′)
        h_y ← Δ(x)
        H_2D(h_x, h_y) ← H_2D(h_x, h_y) + 1
      end if
    end for
```

3.2.2. Maximum bin selection

In the selected candidates, the most representative pixels have the same color information and the highest probability densities. Hence, we select the maximum bin of H_{2D} denoted by

$$H_{2D}^{\max} = \max(H_{2D}). \tag{21}$$

Fig. 3 shows the ultimately determined candidates corresponding to the maximum bin. Compared to Fig. 2(c), it further removes some bright pixels that surround the headlights. Although most of the fog pixels are also removed, it is still capable of computing airlight color via the maintained fog pixels.

3.3. Airlight color computation

We compute the airlight color with the use of the remaining candidates. For each channel, the airlight color can be computed by averaging the color value of the remaining candidates. This computation can be expressed in Algorithm 3.

Algorithm 3. Airlight color computation.

```
(A_0, A_1, A_2) ← (0, 0, 0)
for each pixel x do
  if Y(x) ≥ μ′ − σ′ and Y(x) ≤ μ′ + σ′ then
    h_x ← Y(x) − (μ′ − σ′)
    h_y ← Δ(x)
    if H_2D(h_x, h_y) = H_2D^max then
      for c = 0 to 2 do
        A_c ← A_c + I_c(x)
      end for
    end if
  end if
end for
for c = 0 to 2 do
  A_c ← (A_c / H_2D^max)
end for
```

After generating A_c, it can be supplied to improve various image fog removal methods based on the physical optic model. In this paper, we then implement the embodiments of the HAE method to improve the DCP, MDCP, LCP, and EPHR methods (He et al., 2011; Gibson et al., 2012; Cheng et al., 2012; Shiau et al., 2013).

4. Experimental results

In natural environments, except for the full indoor scenes, image luminance varies with different kinds of weather conditions, such as sunny days, rainy days, foggy days, and so on. In order to estimate the performance of image fog removal, we captured 12 ideal color images in various outdoor scenes. We also use Adobe Photoshop CS6 software to add foggy weather saturation with highlights into those images (denoted by F-01, F-02, F-03, ..., F-12). In our experiments, we perform qualitative evaluation, quantitative assessment, and examination of time complexity in order to compare the performances of the MDCP, LCP, EPHR, and our HAE methods.

4.1. Qualitative evaluation

Figs. 4 and 5 illustrate image fog removal using the different methods. As shown in Fig. 4(a), there are 12 ideal color images captured under different kinds of outdoor scenes. It indicates that the observers can perceive good visual quality from those images. After the fog and highlight are increased in the images indicated in Fig. 4 (b), the luminance, saturation, hue, and other image features are degraded. As shown in Fig. 4(c), when those poor quality images are processed by the MDCP method, the original image features are enhanced, but the output images become very dim due to incorrect airlight estimation. Fortunately, the aforementioned side effects can be easily removed by our HAE method. Hence, after the airlight estimation module of the MDCP method is replaced by our HAE method, the bright output images with acceptable image features can be generated as shown in Fig. 4(d). Similarly, the same side effects are also presented by the LCP and EPHR methods as displayed in Fig. 5(a) and (c). Again, our method appropriately improves the two methods indicated in Fig. 5(b) and (d).

4.2. Quantitative assessment

In order to further verify the effectiveness of our HAE method, we apply the feature similarity (FSIM) metric (Zhang et al., 2011) to assess the output results in Figs. 4 and 5 for quantitative measurement. Note that higher FSIM values denote higher quality. Upon comparing the differences between the defogged images and the ideal images using FSIM, it can be seen that the HAE method can improve the restoration effects of each method as listed in Table 2. After the comparison, we also find that EPHR method provides the better image quality than those by the MDCP and LCP methods. This is because the EPHR simplified the airlight computation using the simple division operator to the maximum luminance value. Hence, the estimated value fortuitously approximates to the airlight, but this improvement effect highly depends on the manual setting of the division value.

Fig. 4. Image fog removal results; (a) ground truth images; (b) images with added fog and highlights; (c) MDCP results; (d) MDCP-HAE results. (For interpretation of the references to color in this figure caption, the reader is referred to the web version of this article.)

4.3. Algorithm complexity

To measure the performance of the proposed HAE method, we analyze its time complexity based on Big-O notation. For an input image that includes B pixels with Y_{length} levels of luma and maximum value Δmax of chroma difference ($|\mathrm{Cb}-\mathrm{Cr}|$), bright region estimation has $O(B+Y_{length})$, and color similarity estimation has $O(B+Y_{length}\times\Delta\mathrm{max})$. However, $Y_{length}\times\Delta\mathrm{max}$ is much lower than B. Therefore, our HAE method belongs to liner time complexity that the computation cost only depends on B.

In addition to Big-O notation, we also report the execution time of each method. Note that all experiments were conducted by Matlab R2014a on a laptop with a 1.80 GHz processor and all methods were executed 100 times to obtain the average time measures. As listed in Table 3, when the HAE method is integrated into MDCP, LCP, and EPHR methods, the overall execution times are not significantly affected. Hence, this indicates that our HAE method is valuable for the improvement of image fog removal without incurring additional computation cost.

5. Conclusions

This paper has proposed a linear time airlight estimation algorithm based on color analysis. Compared to the previous methods that only focus on luminance estimation, the proposed method estimates the color probability in YCbCr space to select candidates of the representative fog pixels for airlight computation. According to qualitative evaluation by visual inspection, quantitative assessment using FSIM metric, Big-O notation, and execution time estimation, we have verified that our proposed method is more effective than the compared methods and has very low

Fig. 5. Image fog removal results; (a) LCP results; (b) LCP-HAE results; (c) EPHR results; (d) EPHR-HAE results.

Table 2
Quantitative measurement using the FSIM metric (Zhang et al., 2011).

Images	MDCP	MDCP-HAE	LCP	LCP-HAE	EPHR	EPHR-HAE
F-01	0.8299	0.9136	0.7565	0.8904	0.8733	0.8964
F-02	0.8351	0.9116	0.7765	0.8865	0.8575	0.8869
F-03	0.8368	0.9126	0.7868	0.8859	0.8753	0.8969
F-04	0.7924	0.9035	0.7482	0.8708	0.8640	0.8941
F-05	0.8005	0.9044	0.7756	0.8779	0.8692	0.8978
F-06	0.8181	0.9084	0.7481	0.8766	0.8697	0.8931
F-07	0.8585	0.9167	0.7914	0.8981	0.8774	0.9011
F-08	0.7835	0.8731	0.7743	0.8780	0.8587	0.8963
F-09	0.8333	0.9055	0.7778	0.8952	0.8699	0.9006
F-10	0.8414	0.8983	0.7663	0.8785	0.8623	0.8846
F-11	0.8354	0.9064	0.8609	0.9267	0.8957	0.9242
F-12	0.7917	0.9002	0.7238	0.8718	0.8611	0.8919
Mean	0.8215	0.9046	0.7739	0.8864	0.8696	0.8970

Table 3
Execution time of each method in seconds.

Images	MDCP	MDCP-HAE	LCP	LCP-HAE	EPHR	EPHR-HAE
F-01	1.401	1.434	2.853	2.768	4.051	4.053
F-02	1.364	1.553	2.817	2.803	4.057	4.056
F-03	1.637	1.588	2.886	2.901	4.103	4.110
F-04	1.391	1.404	2.903	2.879	4.086	4.082
F-05	1.385	1.399	2.664	2.624	4.052	4.053
F-06	1.451	1.486	2.763	2.755	4.061	4.059
F-07	1.481	1.453	2.557	2.617	4.077	4.076
F-08	1.517	1.499	2.781	2.791	4.087	4.081
F-09	1.539	1.518	2.807	2.809	4.062	4.063
F-10	1.603	1.627	2.769	2.771	4.058	4.059
F-11	1.587	1.589	2.911	2.903	4.059	4.057
F-12	1.668	1.653	2.646	2.651	4.063	4.065
Mean	1.502	1.516	2.786	2.772	4.068	4.067

computation cost. In our future work, we will research the effective transmission model module in order to obtain an optimal defogging solution.

Acknowledgement

This work was supported by Ministry of Science and Technology, Taiwan under the research projects 103-2221-E-027-030-MY2 and 103-2221-E-027-031-MY2.

References

Chaudhury, K.N., Sage, D., Unser, M., 2011. Fast $O(1)$ bilateral filtering using trigonometric range kernels. IEEE Trans. Image Process. 20 (December (2)), 3376–3382.

Cheng, F.-C., Lin, C.H., Lin, J.-L., 2012. Constant time $O(1)$ image fog removal using lowest level channel. Electron. Lett. 48 (October (22)), 1404–1406.

Fattal, R., 2008. Single image dehazing. ACM Trans. Graph. 27 (August (3)), 721–729.

Gibson, K.B., Vo, D.T., Nguyen, T.Q., 2012. An investigation of dehazing effects on image and video coding. IEEE Trans. Image Process. 21 (February (2)), 662–673.

Hautiere, N., Tarel, J.-P., Aubert, D., 2010. Mitigation of visibility loss for advanced camera-based driver assistance. IEEE Trans. Intell. Transport. Syst. 11 (June (2)), 474–484.

He, K., Sun, J., Tang, X., 2011. Single image haze removal using dark channel prior. IEEE Trans. Pattern Anal. Mach. Intell. 33 (December (12)), 2341–2353.

Kim, W., Kim, C., 2012. Background subtraction for dynamic texture scenes using fuzzy color histograms. IEEE Signal. Process. Lett. 19 (March (3)), 127–130.

Kopf, J., Neubert, B., Chen, B., Cohen, M., Cohen-Or, D., Deussen, O., Uyttendaele, M., Lischinski, D., 2008. Deep photo: model-based photograph enhancement and viewing. ACM Trans. Graph. 27 (December (5)), 116:1–116:10.

Levin, A., Lischinski, D., Weiss, Y., 2008. A closed-form solution to natural image matting. IEEE Trans. Pattern Anal. Mach. Intell. 30 (February (2)), 228–242.

Middleton, W., 1952. Vision Through the Atmosphere. University Toronto Press, Toronto, ON, Canada.

Narasimhan, S.G., Nayar, S.K., 2003a. Contrast restoration of weather degraded images. IEEE Trans. Pattern Anal. Mach. Intell. 25 (June (6)), 713–724.

Narasimhan, S.G., Nayar, S.K., 2003b. Interactive (de)weathering of an image using physical models. In: ICCV Workshop on Color and Photometric Methods in Computer Vision, pp. 1387–1394.

Otsu, N., 1979. A threshold selection method from gray-level histograms. IEEE Trans. Syst. Man Cybern. 9 (January (1)), 62–66.

Shiau, Y.-H., Yang, H.-Y., Chen, P.-Y., Chuang, Y.-Z., 2013. Hardware implementation of a fast and efficient haze removal method. IEEE Trans. Circuits Syst. Video Technol. 23 (August (8)), 1369–1374.

Shwartz, S., Namer, E., Schechner, Y.Y., 2006. Blind haze separation. In: Proceedings of the IEEE Conference on Computer Vision and Pattern Recognition, vol. 2, pp. 1984–1991.

Tan, R., 2008. Visibility in bad weather from a single image. In: Proceedings of the IEEE Conference on Computer Vision and Pattern Recognition, pp. 1–8.

Wen, Yi., Lu, Y., Yan, J., Zhou, Z., von Deneen, K.M., Shi, P., 2011. An algorithm for license plate recognition applied to intelligent transportation system. IEEE Trans. Intell. Transport. Syst. 12 (September (3)), 830–845.

Yoon, I., Kim, S., Kim, D., Hayes, M.H., Paik, J., 2012. Adaptive defogging with color correction in the HSV color space for consumer surveillance system. IEEE Trans. Consum. Electron. 58 (February (1)), 111–116.

Zhang, L., Zhang, L., Mou, X., Zhang, D., 2011. FSIM: a feature similarity index for image quality assessment. IEEE Trans. Image Process. 20 (August (8)), 2378–2386.

Zou, W.W., Yuen, P.C., Chellappa, R., 2013. Low-resolution face tracker robust to illumination variations. IEEE Trans. Image Process. 22 (May (5)), 1726–1739.